Journal of Biomolecular NMR, **13:** 213–221, 1999.
KLUWER/ESCOM

Heteronuclear relaxation in time-dependent spin systems: ^{15}N-$T_{1\rho}$ dispersion during adiabatic fast passage

Robert Konrat* & Martin Tollinger
Institute of Organic Chemistry, University of Innsbruck, A-6020 Innsbruck, Austria

Received 30 September 1998; Accepted 16 November 1998

Key words: adiabatic fast passage, ^{15}N NMR, heteronuclear relaxation, protein dynamics, $T_{1\rho}$-dispersion

Abstract

A novel NMR experiment comprising adiabatic fast passage techniques for the measurement of heteronuclear self-relaxation rates in fully ^{15}N-enriched proteins is described. Heteronuclear self-relaxation is monitored by performing adiabatic fast passage (AFP) experiments at variable adiabaticity (e.g., variation of RF spin-lock field intensity). The experiment encompasses gradient-selection and sensitivity-enhancement. It is shown that transverse relaxation rates derived with this method are in good agreement with the ones measured by the classical Carr–Purcell–Meiboom–Gill (CPMG) sequences. An application of this method to the study of the carboxyl-terminal LIM domain of quail cysteine and glycine-rich protein qCRP2(LIM2) is presented.

Abbreviations: CPMG, Carr–Purcell–Meiboom–Gill; CSA, chemical shift anisotropy; DD, dipole-dipole; NOE, nuclear Overhauser effect; HSQC, heteronuclear single-quantum correlation spectroscopy; T_1, longitudinal relaxation time; T_2, transverse relaxation time; $T_{1\rho}$, spin-lock relaxation time.

Introduction

Measurement of heteronuclear relaxation rates probes molecular dynamics over a wide time range and provides important insight into the motional behavior of proteins in solution (Peng and Wagner, 1994; Dayie et al., 1996; Palmer et al., 1996). In particular, the relaxation properties of protonated heteronuclei such as ^{15}N or ^{13}C are dominated by the dipole-dipole interaction with the directly attached proton and can be used to efficiently characterize both overall rotational diffusion as well as intramolecular dynamics of proteins and other biomolecules (Dayie et al., 1996). Due to the developments of two-dimensional proton-detected heteronuclear NMR spectroscopy and of efficient biosynthetic methods for isotopic enrichment of proteins, studies of protein dynamics have become a routine method and an integral part of almost every NMR protein structure determination effort.

*To whom correspondence should be addressed. E-mail: robert.konrat@uibk.ac.at.

Every pulse sequence commonly used for measuring ^{15}N or ^{13}C relaxation rates invariably starts with the preparation of the respective non-equilibrium spin state, be it either inverted longitudinal S_z (T_1-measurement) or transverse $S_{x,y}$ (T_2-measurement) magnetization, respectively. After evolving under an effective Hamiltonian and relaxation superoperator during a variable relaxation period, the final spin state is monitored using a two-dimensional proton-detected heteronuclear correlation experiment. Relaxation rates are obtained from an analysis of a time series of cross-peak intensities as a function of relaxation delay. The effective Hamiltonian and relaxation superoperator can be modified by applied radio-frequency fields and pulse sequences have been devised for measurements of spin-lattice relaxation (Kay et al., 1989; Sklenar et al., 1987), spin-spin relaxation (Nirmala and Wagner, 1989; Peng et al., 1991a,b; Kay et al., 1992a; Palmer et al., 1992), heteronuclear nuclear Overhauser effect (Kay et al., 1989), rotating frame relaxation (Peng et al., 1991a,b; Szyperski et al., 1993) and relaxation of two-spin order, both longitudinal and

transverse (Peng and Wagner, 1992). It is well established that cross-correlated cross-relaxation leads to a multi-exponential decay of magnetization (e.g., partial conversion of one-spin order to multi-spin order and vice versa) and can disturb relaxation measurements. Pulse sequences which eliminate these possible pitfalls have been developed (Boyd et al., 1990; Palmer et al., 1992; Kay et al., 1992b).

Dynamic processes on microsecond to millisecond (μs–ms) time scales are probed by a variety of different experimental schemes. The first method consists of measuring the transverse relaxation rate R_2 using a Carr–Purcell–Meiboom–Gill (CPMG) sequence (Carr and Purcell, 1954; Meiboom and Gill, 1958). The dependence of R_2 on the CPMG delay probes exchange rates on the order of $10^3 - 10^4$ Hz (Gutowsky et al., 1965; Orekhov et al., 1994, 1995). The second method is based on $T_{1\rho}$-dispersion measurements (e.g., measurement of the spin-lock relaxation rate $R_{1\rho}$ as a function of the radiofrequency spin-lock amplitude) (Deverell et al., 1970; Brüschweiler and Ernst, 1992; Peng and Wagner, 1992; Szyperski et al., 1993). Recently, the range of exchange rates detectable by this method was extended by performing the relaxation rate measurements along an effective field axis tilted by an angle θ away from the static magnetic field axis (Desvaux et al., 1995; Zinn-Justin et al., 1997; Akke and Palmer, 1996; Mulder et al., 1998; Akke et al., 1998).

The inevitable problem of rf inhomogeneity in NMR has led to the introduction of adiabatic fast passage (AFP) (Abragam, 1986) into high resolution NMR spectroscopy (Böhlen and Bodenhausen, 1993; Kupce and Freeman, 1995). This was largely the result of the fact that these pulses have outstanding inversion profiles over large frequency as well as the extremely beneficial property that the inversion performance is not sensitive to the exact radiofrequency level provided that the adiabatic condition is full-filled, i.e. that the magnetization vector follows the time-dependent effective field $\omega_{eff}(t)$ (Abragam, 1986) (Figure 1). The rf amplitudes of such pulses can be apodized at the beginning and the end so that complete inversion of the magnetization is ensured. Recently a more sophisticated application of such pulses to studies of differentially labeled molecular complexes has been reported (Zwahlen et al., 1997). In this experiment, use was made of the fact that the respective times of inversion are different for spins resonating with different chemical shifts when sweeping the rf carrier through the spectrum. Based on the roughly linear $^1J_{CH}$ vs chemical shift profile the magnetization transfer for different CH spin pairs could be independently optimized, which led to an improved purging efficiency of unwanted signals in NOESY spectra.

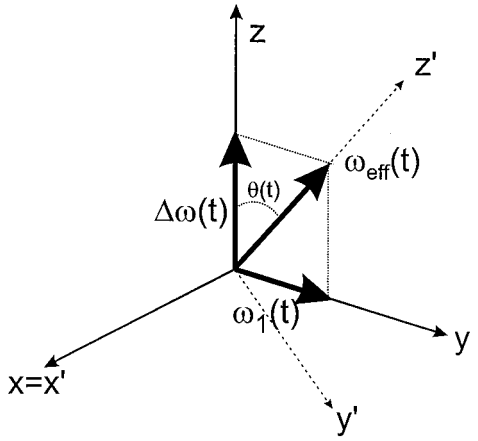

Figure 1. Representation of the adiabatic spin-lock frame. The x,y,z reference frame is rotating with the S spin carrier frequency. The x′,y′,z′ spin-lock frame is tilted so that z′ points along the direction of the effective field $\omega_{eff}(t)$, defined as the vector sum of the rf amplitude $\omega_1(t)$ and the offset $\Delta\omega(t)$. During the time course of the adiabatic fast passage z′ moves gradually from z to −z, passing y exactly at on-resonance.

In this paper a different application of adiabatic inversion pulses (adiabatic fast passage) is demonstrated. Spin inversion by adiabatic fast passage is typically accomplished using adiabatic frequency sweeps which are very large compared with the radio-frequency field intensity (expressed in frequency units) and hence it is commonly assumed that spin inversion occurs at the point where the adiabatic frequency sweep passes through the chemical shift of a given spin. Relaxation during the adiabatic fast passage is therefore mainly longitudinal. In contrast, if the radio-frequency field intensity is comparable to the frequency sweep range, significant transverse magnetization will be created. At a given sweep rate, different net amounts of transverse magnetization during the time course of the adiabatic inversion pulse can be created by a variation of the rf amplitude. This leads to a different *effective* relaxation rate (adiabatic spin-lock frame relaxation rate $R_{1\rho}$), which is given as the weighted average of longitudinal and transverse relaxation. In this article, we demonstrate the measurement of transverse (R_2) relaxation rates based on nuclear magnetic relaxation during adiabatic fast passage at variable rf amplitudes. Given the fact that these adiabatic pulses are less sensitive to

rf field inhomogeneity than conventional (π) pulses, the relaxation rates obtained are less prone to systematic errors. As a first example, the new adiabatic spin-lock frame relaxation experiment is applied to the fully ^{15}N-enriched carboxyl-terminal LIM domain qCRP2(LIM2) of quail cysteine- and glycine-rich protein CRP2, a protein involved in cell growth and differentiation (Weiskirchen et al., 1995).

Materials and methods

Uniformly ^{15}N-labeled carboxyl-terminal LIM domain qCRP2(LIM2) of quail cysteine- and glycine-rich protein CRP2 was prepared and purified as described previously. Signal assignment and structural data of qCRP2(LIM2) have already been published (Konrat et al., 1997).

All NMR experiments were performed on a Varian UNITY Plus 500 MHz spectrometer equipped with a pulsed field gradient (PFG) unit using a triple resonance probe with actively shielded z gradients. The sample contained 3.0 mM of ^{15}N-labeled qCRP2(LIM2), as well as 20 mM potassium phosphate buffer pH 7.2, 50 mM KCl and 0.5 mM dithiothreitol in 90% H_2O/10% D_2O. All spectra were recorded at 26 °C. All experiments performed used spectral widths of 1650×8000 Hz in the $t_1 \times t_2$ dimensions. The ^{1}H carrier was set to the frequency of the water resonance (4.76 ppm), and the ^{15}N carrier frequency was set to 116 ppm. Decoupling of ^{15}N spins during acquisition was performed using the WURST decoupling scheme (Kupce and Freeman, 1995) with a decoupling power of $\gamma B_1 = 900$ Hz.

^{15}N-T_1 and ^{15}N-T_2 experiments (reference experiments). Longitudinal and transverse relaxation times for the ^{15}N nuclei of qCRP2(LIM2) were determined by two-dimensional, proton detected sensitivity-enhanced NMR experiments (Farrow et al., 1994) using inversion recovery and CPMG pulse schemes, respectively. All spectra were recorded as 64×512 complex matrices with 32 scans per complex t_1 point. Recycle delays of 1 s were employed in both the ^{15}N–T_1 and ^{15}N–T_2 experiment. The T_1 experiment was recorded with six delays of 0.0, 166.5, 333.0, 499.5, 666.0 and 832.5 ms, while the seven delays in the T_2 experiment were 0.0, 15.7, 31.4, 47.1, 62.8, 78.5 and 94.2 ms. In the CPMG pulse sequence, the ^{15}N 90 degree pulse length was 69 μs, corresponding to a power level of 3.6 kHz.

AFP experiment. For the determination of adiabatic spin lock relaxation times the sequence in Figure 2 was used. The length of the adiabatic fast passage rf pulse was 100 ms, a frequency range of 2000 Hz was chosen, corresponding to a sweep rate of 2×10^4 s^{-2}. The middle of the frequency sweep was adjusted to 116 ppm. Numerical simulations (neglecting cross-relaxation and additional remote scalar coupling) of the outcome of this adiabatic fast passage show that perfect inversion occurs within the spectral range 116 ± 15 ppm (at 500 MHz). The shape of the rf pulse consisted of 1024 complex points.

Seventeen experiments were performed varying the rf amplitude during the 100 ms AFP delay using the following values: 0, 159, 172, 200, 217, 238, 278, 305, 347, 385, 438, 481, 595, 649, 714, 794 and 960 Hz. Experiments with amplitudes set to 159 Hz, 385 Hz and 960 Hz were repeated to assess the reproducibility of the method. In addition, a reference experiment using the same pulse scheme (Figure 2) but with the length of the AFP delay set to 0 ms was performed. Rf amplitudes were experimentally determined by calibrating on-resonance 180 degree pulses at the respective power levels using a sample of ^{15}N-labeled benzamide. The WALTZ-16 (Shaka et al., 1983) decoupling power was set to 6250 Hz, corresponding to a nominal 90 degree flip angle of 40 μs. All spectra were recorded as 64×512 complex matrices with 32 scans per complex t_1 point, and a repetition delay between scans of 1 s was used in all experiments.

Data processing. NMR data were processed using NMRPipe software (Delaglio, 1993). All spectra were linearly predicted in t_1, weighted with a phase-shifted sine bell in t_1 and t_2, and zero-filled in each dimension prior to Fourier transformation. Peak volumes were measured using Felix software (Biosym/MSI, 1995). ^{15}N–T_1 and ^{15}N–T_2 values were determined by non-linear least-squares fitting of the experimental data from the inversion recovery and CPMG experiments to two parameter monoexponential equations. For the AFP experiment, ^{15}N–T_2 values were determined by linear least-squares fits of the effective spin lock relaxation rates $R_{1\rho}$ to $\sin^2 \theta_{eff}$ using the longitudinal relaxation rates ^{15}N–T_1 from the conventional inversion recovery experiment.

Adiabatic fast passage

The sequence for measuring the adiabatic spin-lock frame relaxation rates derives from the ^{15}N longi-

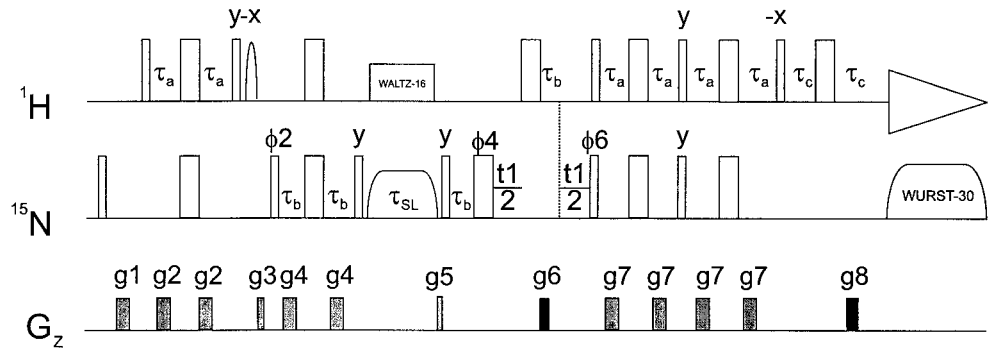

Figure 2. Pulse scheme used for the measurement of ^{15}N adiabatic spin-lock frame relaxation. Narrow and wide pulses indicate 90° and 180° pulses, respectively, darker gradients indicate those used for coherence transfer selection, and, unless indicated otherwise, all pulses are applied along the x-axis. The water-selective ^{1}H 90° pulse is applied as a 2.2 ms rectangular pulse, with the carrier on the water resonance. The values for τ_a, τ_b and τ_c were set to 2.25 ms, 2.75 and 0.75 ms, respectively. Gradient levels were as follows: g1=1.0 ms, 5 Gcm^{-1}; g2=0.5 ms, 4 Gcm^{-1}; g3=1.0 ms, 10 Gcm^{-1}; g4=0.5 ms, 8 Gcm^{-1}; g5=1.0 ms, 25 Gcm^{-1}; g6=1.25 ms, 30 Gcm^{-1}; g7=0.5 ms, 4 Gcm^{-1} and g8=0.125 ms, 29 Gcm^{-1}. The phase cycling was $\phi2$ = x,−x; $\phi4$=2(x),2(y),2(-x),2(-y); $\phi6$=x; and receiver was x,−x,−x,x. For each increment of t_1, two FIDs were collected with the phase of $\phi6$ and the amplitude of g6 inverted in the second FID.

tudinal self-relaxation rate experiment described by Kay and co-workers (Farrow et al., 1994) (Figure 2). It comprises water flip-back pulses in order to minimize saturation of amide proton signals due to transverse water magnetization (Grzesiek and Bax, 1993), as well as gradient-selection combined with sensitivity-enhancement (Cavanagh et al., 1991; Palmer et al., 1991; Kay et al., 1992b). However, instead of the relaxation delay in the ^{15}N–T_1 experiment an adiabatic fast passage with variable rf field intensity is performed. This is achieved by an amplitude and phase-modulated radio-frequency pulse. The frequency sweep results from a parabolic phase modulation of the pulse. The B_1 field is kept constant throughout the majority of the pulse with the exception of the edges, where the B_1 field is ramped from zero to ω_1^{max} and from ω_1^{max} to zero during the first and last fractions of the pulse (typically ≈30%), respectively (Zwahlen et al., 1997). This ensures that the magnetization is placed along the −z axis at the end of inversion, whereas in the case of a constant B_1 field the effective field and hence the magnetization is aligned at a certain angle different from 0 or π, even at large frequency sweeps. In the sequence of Figure 2, relaxation induced by the cross-correlation between DD and CSA interactions (Boyd et al., 1990) is suppressed using the WALTZ-16 decoupling scheme (Shaka et al., 1983), as in ^{15}N–T_1 and ^{15}N–T_2 measurements, respectively.

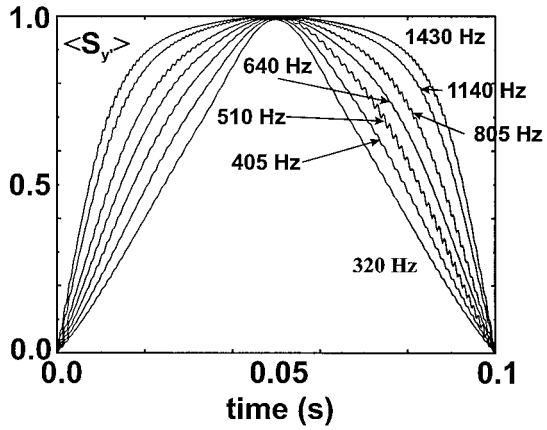

Figure 3. Simulation of the time evolution of the expectation values for transverse magnetization $\langle S_{y'} \rangle$ during the adiabatic fast passage, demonstrating the effect of increasing the rf amplitude. The following parameters were used: duration of adiabatic sweep = 100 ms, sweep of 2.0 kHz, sweep rate = 2×10^4 s^{-2}, apodization of the first and last 30% using a sine function, pulse duration 100 ms, the center of the sweep coincides with the resonance frequency of spin S. Rf amplitudes used in the simulations were: 320, 405, 510, 640, 805, 1140 and 1430 Hz.

Theory

Figure 3 shows the time-evolution of transverse $\langle S_{y'} \rangle$ magnetization during adiabatic fast passages at variable rf amplitudes. The adiabatic spin-lock frame relaxation rate can effectively be calculated following well-established approaches for describing nuclear spin relaxation in the presence of time-dependent perturbations (Griesinger and Ernst, 1988). In what follows, it is assumed that the the longest correlation time

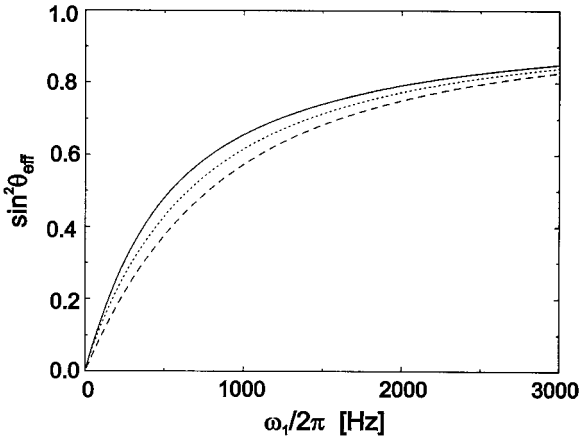

Figure 4. Profile of $\sin^2\theta_{eff}$ vs ω_1 as a function of offset. The offset is defined as the difference between the S spin resonance frequency and the center of the adiabatic frequency sweep (on-resonance, solid line; 250 Hz, dotted line; 500 Hz, dashed line). The parameters for the adiabatic frequency sweep were identical to those of Figure 3.

τ_{corr} of the random processes that cause relaxation is on the order of nanoseconds and that the superoperator is not affected by the radio-frequency pulse. In the case of an adiabatic frequency sweep, this is justified as the condition $\omega_{eff} \ll 1/\tau_{corr}$ is always fulfilled. The time-dependent adiabatic spin-lock frame self-relaxation rate $R_{SL}(t)$ of the ^{15}N magnetization aligned with the time-dependent effective field is then given by

$$R_{SL}(t) = \cos^2\theta(t)R_1 + \sin^2\theta(t)R_2 \quad (1)$$

where R_1 and R_2 are the longitudinal and transverse relaxation rates. $\theta(t)$ is the time-dependent tilt angle (see Figure 1). This equation can be linearized in $\sin^2\theta(t)$ to result in

$$R_{SL}(t) = R_1 + \sin^2\theta(t)\{R_2 - R_1\} \quad (2)$$

If the decay of $\langle S_{z'}\rangle$ is purely mono-exponential, the effective adiabatic spin-lock frame relaxation rate $R_{1\rho}$ is given by

$$R_{1\rho} = R_1 + \{R_2 - R_1\}1/\tau_p \int \sin^2\theta(t)dt \quad (3)$$

or (after integration)

$$R_{1\rho} = R_1 + \{R_2 - R_1\}\sin^2\theta_{eff} \quad (4)$$

where θ_{eff} is the effective tilt angle. The intensity after the adiabatic fast passage of duration τ_p, $I(\tau_p)$, is given by

$$I(\tau_p) = I(0)\exp[-R_{1\rho} * \tau_p] \quad (5)$$

Equation 5 can be used to determine the effective adiabatic spin-lock frame relaxation rate $R_{1\rho}$ by measuring the residual ^{15}N magnetization. The value of $\sin^2\theta_{eff}$ can be calculated numerically as all the parameters governing the effective tilt angle are defined (e.g., sweep rate and rf amplitude). The exact value of $\sin^2\theta_{eff}$ can be chosen at will by the experimentalist, limited only by the rf amplitude requirement for adiabatic inversion and by hardware parameters (e.g., probe safety precautions). Figure 4 shows simulations of $\sin^2\theta_{eff}$ as a function of rf amplitude ω_1(for different resonance frequencies). At a given sweep rate, $\sin^2\theta_{eff}$ can be modified in a straightforward manner by simply varying the rf amplitude of the frequency sweep. The linear dependence of the effective adiabatic spin-lock frame relaxation rate $R_{1\rho}$ vs $\sin^2\theta_{eff}$ can then be used to extract longitudinal (R_1) and transverse (R_2) relaxation rates from a rf amplitude series. The linear relationship between $R_{1\rho}$ and $\sin^2\theta_{eff}$ is outlined in the simulations of Figure 5B, with the curves calculated using Equation 5.

Results and discussion

Figure 2 illustrates the pulse scheme which was used to measure the adiabatic spin-lock frame relaxation rates for the backbone amide nitrogens of the carboxyl-terminal LIM domain qCRP2(LIM2) from quail cysteine- and glycine-rich protein CRP2. In sum, 17 experiments were performed varying the rf amplitude during the 100 ms adiabatic fast passage delay between 0 and 960 Hz, as well as a reference experiment using the same pulse scheme but with the length of the AFP delay set to 0 ms. The lower limit of the dispersion profile or rf amplitude is marked by the minimal value for the rf amplitude, which is necessary to fulfill the adiabatic condition ($\omega_{eff} \gg d\theta/dt$) (Abragam, 1986), which in turn is dependent on the sweep rate and the duration of the frequency sweep. In this case the magnetization is not effectively locked but instead nutates around the effective field. Hence, at the end of the adiabatic frequency sweep the magnetization is not perfectly aligned along the effective field (e.g. inverted), which leads to an overestimation of the experimentally determined decay rate $R_{1\rho}$. The upper limit of rf amplitude is simply determined by spectrometer hardware (e.g., the safety criteria of the probe). Evolution under the one-bond heteronuclear scalar coupling $^1J_{NH}$ does not have to be consid-

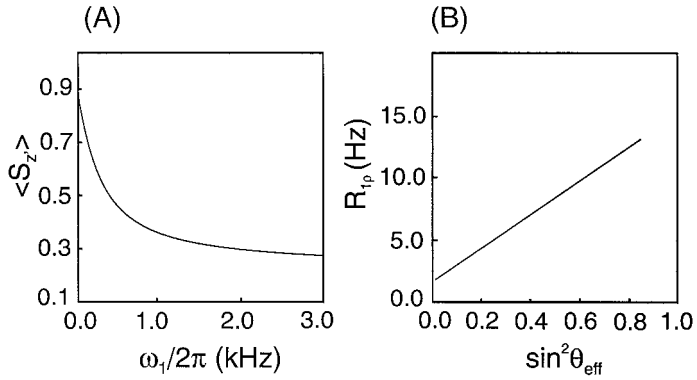

Figure 5. Simulation of the outcome of an adiabatic fast passage (AFP) dispersion experiment for a heteronuclear spin system. (A) ω_1 dependence of the expectation value for longitudinal magnetization $\langle S_{z'} \rangle$, (B) $R_{1\rho}$ vs $\sin^2 \theta_{eff}$ profiles. The following parameters were used: sweep width 2.0 kHz, sweep rate $= 2 \times 10^4$ s^{-2}, apodization of the first and last 30% using a sine function, pulse duration 100 ms, the center of the sweep coincides with the resonance frequency of spin S. $\sin^2 \theta_{eff}$ was obtained from a numerical integration of $\sin^2 \theta(t)$ decomposing the spin lock into 2000 time intervals. The following relaxation rates were used: $R_1 = 1.67$ s^{-1}; $R_2 = 16.7$ s^{-1}. At $\omega_1 = 0$, $\langle S_{z'} \rangle$ is not equal to the equilibrium intensity because of longitudinal relaxation during the time of the adiabatic sweep.

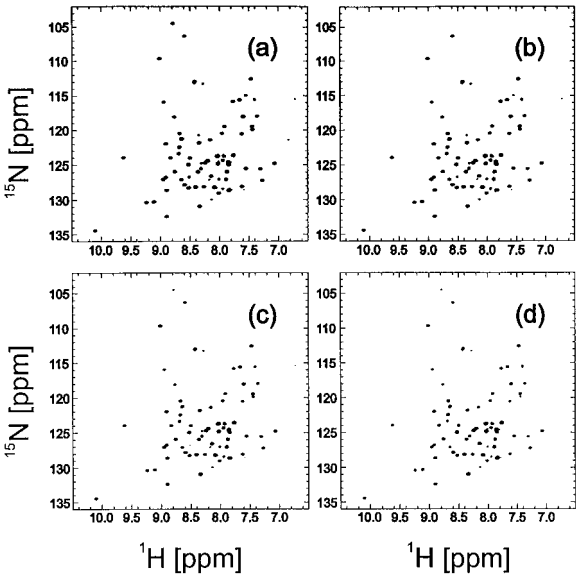

Figure 6. Two-dimensional ^{15}N-^{1}H correlation spectra obtained from a sample of fully ^{15}N-enriched qCRP2(LIM2), recorded with the pulse sequence of Figure 2 used to determine the relaxation rates $R_{1\rho}$ during adiabatic fast passage. For these spectra, the rf amplitudes during adiabatic fast passage were set to 0 Hz (a), 159 Hz (b), 385 Hz (c) and 960 Hz (d).

ered, as ^{1}H-decoupling is applied during the adiabatic frequency sweep.

Figure 6 shows typical spectra obtained with the pulse sequence of Figure 2, demonstrating the quality of the recorded data. No extensive water subtraction or baseline correction routines were necessary. The effective spin-lock relaxation rates $R_{1\rho}$ were determined from residual signal intensities according to Equation 5. Representative linearized plots of the experimentally determined effective spin-lock relaxation rates $R_{1\rho}$ vs $\sin^2 \theta_{eff}$ are shown in Figure 7B. The transverse (R_2) relaxation rates were determined by a linear least-squares fit of the effective spin-lock relaxation rate $R_{1\rho}$ to $\sin^2 \theta_{eff}$, which was obtained from the time integral of $\sin^2 \theta(t)$ (see also Figure 4), using longitudinal relaxation rates obtained from a conventional inversion-recovery experiment. The simultaneous extraction of longitudinal (R_1) relaxation rates from the $T_{1\rho}$ dispersion profile resulted in a less satisfactory agreement. In the AFP experiment, there was a systematic overestimation of the relaxation rate in the experiment for $\gamma B_1 = 0$ Hz spin lock field strength, presumably due to ^{1}H decoupling during the longitudinal relaxation delay. In addition, rotating-frame relaxation rates $R_{1\rho}$ obtained at low spin lock amplitudes might be prone to small errors due to the violation of the adiabatic condition ($\omega_{eff} \gg d\theta/dt$) (Abragam, 1986). Since the accuracy of the transverse relaxation rates R_2 obtained from the slope of the $R_{1\rho}$ vs $\sin^2 \theta_{eff}$ profile in the AFP experiment strongly depends on accurate R_1 values, we prefer (and suggest) to use R_1 values from inversion-recovery experiments. RF inhomogeneity should not introduce significant errors in the AFP obtained T_2 values. From inspection of Figure 4, it can be seen that a distribution of the spin lock amplitude results in an almost symmetric distribution of $\sin^2 \theta_{eff}$ around the true value of $\sin^2 \theta_{eff}$. However, the average $\sin^2 \theta_{eff}$ value (e.g., average value over the probe volume) should be close to the theoretical

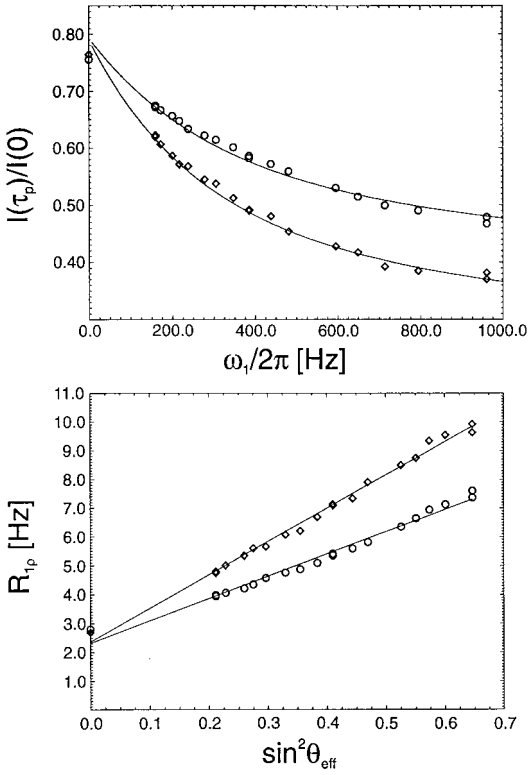

Figure 7. Experimental adiabatic fast passage results for residues Tyr[128] (circles) and Asn[165] (squares) in qCRP2(LIM2). Top: Representative relaxation curves for the adiabatic fast passage dispersion experiment. The decays were monitored using 17 different rf amplitudes (see text for details); experiments at rf amplitudes set to 159 Hz, 385 Hz and 960 Hz were repeated. Superimposed are best-fit dispersion curves using R_1 and R_2 parameters obtained from a linear least-squares regression analysis of Equation 4. Note that intensities are referenced to an experiment with the length of the AFP delay set to 0 ms. Thus, at $\gamma B_1/2\pi = 0$, the residual intensity is not equal to the equilibrium intensity because of longitudinal relaxation during the time of the adiabatic sweep. Bottom: Experimental effective adiabatic spin-lock frame relaxation rate $R_{1\rho}$ vs $\sin^2\theta_{eff}$ profiles; the solid lines drawn are fits to the data.

value and thus the slope in the $R_{1\rho}$ vs $\sin^2\theta_{eff}$ profile (Equation 4) should be almost unaffected. This is in contrast to the CPMG-technique where RF inhomogeneity results in 180° pulse imperfections and altered decay rates.

To assess the procedure using $T_{1\rho}$ dispersion during adiabatic fast passage for ^{15}N self-relaxation time measurements, the obtained transverse ^{15}N relaxation times have been compared to values based on a conventional ^{15}N-T_2 experiment. For the comparison only those residues have been considered which displayed resolved cross peaks in the two dimensional ^{1}H-^{15}N correlation spectra. There is a convincing correlation

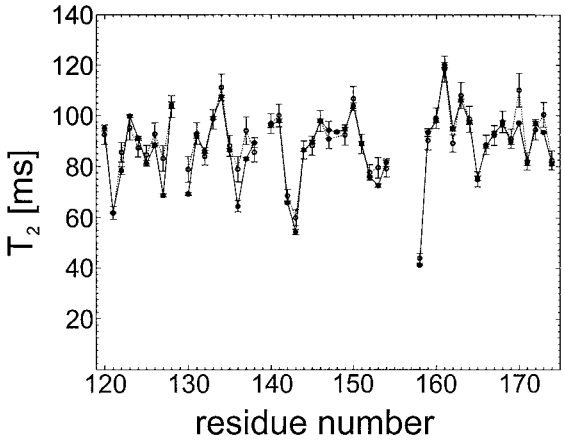

Figure 8. Residue plot showing a comparison of the transverse ^{15}N relaxation times (^{15}N-T_2) in qCRP2(LIM2) obtained by $T_{1\rho}$ dispersion during adiabatic fast passage (open circles/dotted lines) and conventional CPMG (filled circles/full lines) experiments. In the case of the adiabatic fast passage experiment, the values of T_2 were obtained by a fit with Equation 4 with longitudinal relaxation times (T_1) obtained from a conventional inversion recovery experiment.

between conventionally determined transverse relaxation times and those obtained with the adiabatic fast passage technique, thus corroborating the reliability of the method (see Figure 8). The correlation coefficient between experimental T_2 values obtained with CPMG or AFP is 0.95 and the weighted root mean square deviation from a line of slope unity is 0.003. However, notable deviations were found for the following residues: Arg[122], Val[127], Ala[130], Ala[136], Gly[137], Asn[143], Ser[153], Gly[170] and Ala[173]. Reduced transverse relaxation rates were found for these residues in the adiabatic fast passage dispersion experiment. This is in agreement with theory, if slow conformational exchange processes are present. Thus, the slight but significant increase in the T_2 values obtained with the AFP experiment is caused by a (partial) quenching of conformational exchange contributions in the adiabatic spin-lock frame. Disregarding these residues from the analysis significantly improves both the correlation coefficient (0.98) and the root mean square deviation (0.0019). The spatial distributions of these residues displaying significant T_2 differences are given in Figure 9. They are mainly located in loop regions connecting secondary structure elements (Val[127], Ala[130], Ala[136], Gly[137] and Ser[153]) or at the beginning (Gly[170]) or at the end of secondary structure elements (Ala[173]), respectively. Particularly interesting are residues Arg[122], Asn[143] and Gly[170]. These residues are part of rubredoxin type turns connecting

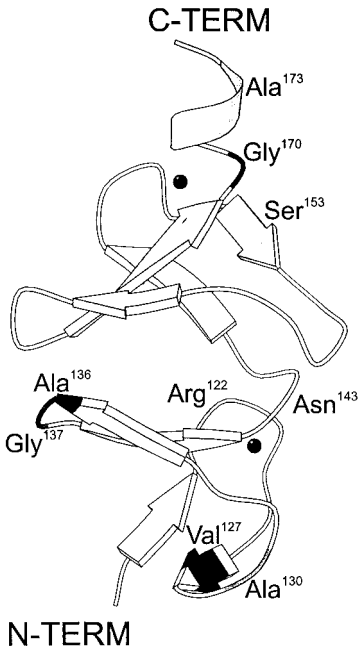

Figure 9. Schematic representation of the spatial distribution of residues in qCRP2(LIM2) displaying significant differences between T_2 values from a conventional CPMG experiment and T_2 values obtained from the AFP technique, respectively. Residues for which notable transverse relaxation rate differences were found are labeled and highlighted in gray (light gray: 5 ms $\leq \Delta T_2 <$ 10 ms; dark gray: $\Delta T_2 \geq 10$ ms). The two central zinc ions of qCRP2(LIM2) are shown as dark spheres. The figure was prepared using the program MOLSCRIPT (Kraulis, 1991).

anti-parallel β-sheets ('Rd-knuckles') and comprising the zinc-coordinating cysteine and histidine residues, respectively (Konrat et al., 1997). Similar conformational flexibility for residues involved in zinc binding or adjacent to zinc coordinating residues were found, for example, within the zinc finger DNA binding domain of *E. coli* Ada (Habazettl et al., 1996). In order to analyze these residues, of course, a more rigorous treatment of conformational exchange contributions is necessary to extract relaxation data from adiabatic $T_{1\rho}$ dispersion curves.

Conclusions

We have presented a novel method to study ^{15}N relaxation in fully ^{15}N-enriched proteins using $T_{1\rho}$ dispersion measurements during adiabatic fast passage (AFP). The experiment derives from a conventional ^{15}N T_1 experiment, in which the longitudinal relaxation delay is replaced by an adiabatic frequency sweep. It also comprises pulsed-field gradients, water flip-back pulses in combination with the enhanced sensitivity method and generates spectra that are free of artifacts. It was demonstrated that transverse relaxation rates obtained with the new pulse scheme are in very good agreement with values obtained from conventional Carr–Purcell–Meiboom–Gill (CPMG) experiments. Given the fact that adiabatic frequency sweeps are used for monitoring the relaxation decay of ^{15}N magnetization, systematic errors due to RF inhomogeneity should be less severe in this experiment and should therefore increase the reliability of the extracted motional parameters. Interpretation of the results was facilitated by the fact that an effective tilt angle θ_{eff} could be defined and relaxation rates $R_{1\rho}$ were extracted from a linear least square fit of the adiabatic spin-lock frame relaxation rates $R_{1\rho}$ vs $\sin^2 \theta_{\text{eff}}$. Microsecond-millisecond time scale motions introduce a non-linear dependence of the effective relaxation rate $R_{1\rho}$ on $\sin^2 \theta_{\text{eff}}$ and the experiment may therefore be used also as a qualitative probe to detect the presence of slow conformational exchange processes.

In sum, we have shown that monitoring nuclear spin relaxation in an adiabatic spin-lock frame provides an efficient means to measure transverse self-relaxation rates. The particularly attractive extension of this method to initial spin states other than longitudinal one-spin order is straightforward and hence extraction of relaxation rates of different transverse multi-spin orders and/or multiple-quantum coherences can be obtained by this technique. Moreover, the technique is not limited to self-relaxation rate measurements but can easily be extended to studies of cross-relaxation processes. By independent variation of the sweep rates and rf amplitudes of the adiabatic frequency fields in heteronuclear spin systems, well-defined effective tilt angles and differences between effective tilt angles can be achieved during the adiabatic spin-lock period. This possibility significantly enriches the prospects of rotating frame relaxation experiments to study self-relaxation, cross-relaxation as well as cross-correlated cross-relaxation pathways of nuclear spin systems. Preliminary explorations of the possible applications are currently under investigation. Given the attractive properties of adiabatic rf pulse schemes, we anticipate that adiabatic spin-lock relaxation measurements will provide a rich avenue to dynamical studies of biologically important molecules.

Acknowledgements

The authors thank Prof. Klaus Bister, Dr Ralf Weiskirchen and Christian Eichmüller (University of Innsbruck) for a sample of fully ^{15}N-enriched qCRP2(LIM2). R.K. thanks Prof. Bernhard Kräutler (University of Innsbruck) for his enthusiastic support and encouragement and Prof. Lewis E. Kay (University of Toronto) for inspiring conversations and delightful discussions. This work was supported by grant P 11600 (Prof. Bernhard Kräutler) from the Austrian Science Foundation FWF.

References

Abragam, A. (1986) *The Principles of Nuclear Magnetism*, Clarendon Press, Oxford, U.K.

Akke, M. and Palmer, A.G. (1996) *J. Am. Chem. Soc.*, **118**, 911–912.

Akke, M., Liu, J., Cavanagh, J., Erickson, H.P. and Palmer, A.G. III (1998) *Nat. Struct. Biol.*, **5**, 55–59.

Biosym/MSI (1995) *Felix User Guide, Version 95.0*, San Diego, CA, U.S.A.

Böhlen, J.M. and Bodenhausen, G. (1993) *J. Magn. Reson. Ser. A*, **102**, 293–301.

Boyd, J., Hommel, U. and Campbell, I.D. (1990) *Chem. Phys. Lett.*, **175**, 477–482.

Brüschweiler, R. and Ernst, R.R. (1992) *J. Chem. Phys.*, **96**, 1758–1766.

Carr, H.Y. and Purcell, E.M. (1954) *Phys. Rev.*, **94**, 630–638.

Cavanagh, J., Palmer, A.G., Wright, P.E. and Rance, M. (1991) *J. Magn. Reson.*, **91**, 429–436.

Dayie, K.T., Wagner, G. and Lefèvre, J.-F. (1996) *Annu. Rev. Phys. Chem.*, **47**, 243–282.

Delaglio, F., Grzesiek, S., Vuister, G., Zhu, G., Pfeifer, J. and Bax, A. (1993) *J. Biomol. NMR*, **6**, 277–293.

Deverell, C., Morgan, R.E. and Strange, J.H. (1970) *Mol. Phys.*, **18**, 553–559.

Desvaux, H., Birlirakis, N., Wary, C. and Berthault, P. (1995) *Mol. Phys.*, **86**, 1059–1073.

Farrow, N.A., Muhandiram, R.D., Singer, A.U., Pascal, S.M., Kay, C.M., Gish, G., Shoelson, S.E., Pawson, T., Forman-Kay, J.D. and Kay, L.E. (1994) *Biochemistry*, **33**, 5984–6003.

Griesinger, C. and Ernst, R.R. (1988) *Chem. Phys. Lett.*, **152**, 239–247.

Grzesiek, S. and Bax, A. (1993) *J. Am. Chem. Soc.*, **115**, 12593–12594.

Gutowsky, H.S., Vold, R.L. and Wells, E.J. (1965) *J. Chem. Phys.*, **43**, 4107–4125.

Habazettl, J., Myers, L.C., Yuan, F., Verdine, G.L. and Wagner, G. (1996) *Biochemistry*, **35**, 9335–9348.

Kay, L.E., Torchia, D.A. and Bax, A. (1989) *Biochemistry*, **28**, 8972–8979.

Kay, L.E., Nicholson, L.K., Delaglio, F., Bax, A. and Torchia, D.A. (1992a) *J. Magn. Reson.*, **97**, 359–375.

Kay, L.E., Keifer, P. and Saarinen, T. (1992b) *J. Am. Chem. Soc.*, **114**, 10663–10665.

Konrat, R., Weiskirchen, R., Kräutler, B. and Bister, K. (1997) *J. Biol. Chem.*, **272**, 12001–12007.

Kraulis, P.J. (1991) *J. Appl. Crystallogr.*, **24**, 946–950.

Kupce, E. and Freeman, R. (1995) *J. Magn. Reson. Ser. A*, **115**, 273–276.

Meiboom, S. and Gill, D. (1958) *Rev. Sci. Instrum.*, **29**, 688–691.

Mulder, F.A.A., de Graaf, R.A., Kaptein, R. and Boelens, R. (1998) *J. Magn. Reson.*, **131**, 351–357.

Nirmala, N.R. and Wagner, G. (1989) *J. Magn. Reson.*, **82**, 659–661.

Orekhov, V.Y., Pervushin, K.V. and Arseniev, A.S. (1994) *Eur. J. Biochem.*, **219**, 887–896.

Orekhov, V.Y., Pervushin, K.V., Korzhnev, D.M. and Arseniev, A.S. (1995) *J. Biomol. NMR*, **6**, 113–122.

Palmer, A.G. III, Cavanagh, J., Wright, P.E. and Rance, M. (1991) *J. Magn. Reson.*, **93**, 151–170.

Palmer, A.G. III, Skelton, N.J., Chazin, W.J., Wright, P.E. and Rance, M. (1992) *Mol. Phys.*, **75**, 699–711.

Palmer, A.G. III, Williams, J. and McDermott, A. (1996) *J. Phys. Chem.*, **100**, 13293–13310.

Peng, J.W., Thanabal, V. and Wagner, G. (1991a) *J. Magn. Reson.*, **95**, 421–427.

Peng, J.W., Thanabal, V. and Wagner, G. (1991b) *J. Magn. Reson.*, **94**, 82–100.

Peng, J.W. and Wagner, G. (1992) *J. Magn. Reson.*, **98**, 308–332.

Peng, J.W. and Wagner, G. (1994) *Methods Enzymol.*, **239**, 563–596.

Shaka, A.J., Keeler, J. and Freeman, R. (1983) *J. Magn. Reson.*, **53**, 313–340.

Sklenar, V., Torchia, D.A. and Bax, A. (1987) *J. Magn. Reson.*, **73**, 375–379.

Szyperski, T., Luginbühl, P., Otting, G., Güntert, P. and Wüthrich, K. (1993) *J. Biomol. NMR*, **3**, 151–164.

Weiskirchen, R., Pino, J.D., Macalma, T., Bister, K. and Beckerle, M.C. (1995) *J. Biol. Chem.*, **270**, 28946–28954.

Zinn-Justin, S., Berthault, P., Guenneugues, M. and Desvaux, H. (1997) *J. Biomol. NMR*, **10**, 363–372.

Zwahlen, C., Legault, P., Vincent, S.J.F., Greenblatt, J., Konrat, R. and Kay, L.E. (1997) *J. Am. Chem. Soc.*, **119**, 6711–6721.